Electronic Supplementary Material (ESI) for Physical Chemistry Chemical Physics.

Fluorescent DNA Probes at Liquid/Liquid Interfaces Studied by Surface Second Harmonic Generation

Giuseppe L. Licari[§], *Pierre-François Brevet*[†], *Eric Vauthey*[§*]

§ Department of Physical Chemistry, University of Geneva, 30 Quai Ernest-Ansermet, CH-1211 Geneva 4, Switzerland.

† Institut Lumière Matière, UMR CNRS 5306, Université Claude Bernard, Lyon 1, Campus LyonTech – La Doua, 10 Rue Ada Byron, 69622 Villeurbanne cedex, France.

* Corresponding Author: eric.vauthey@unige.ch

1. Additional SSHG spectra

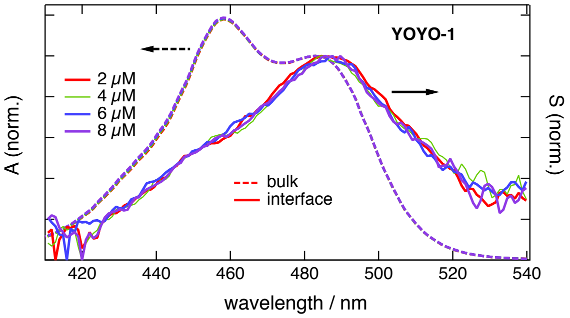

Figure S1. Absorption and SSHG spectra, $S(\lambda)$, measured with different concentrations of YOYO-1 in PBS and at the dodecane/PBS interface.

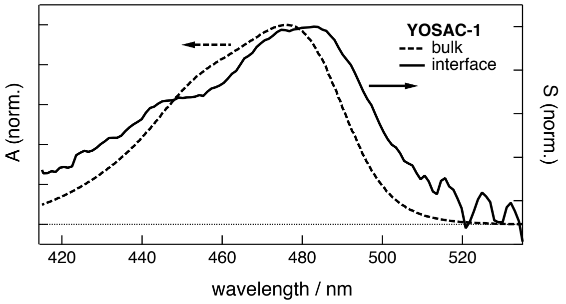

Figure S2. Electronic absorption and SSHG spectra, $S(\lambda)$, measured with YOSAC-1 (5 μM) in PBS and at the dodecane/PBS interface.

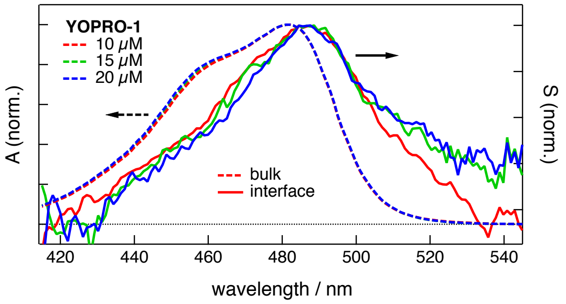

Figure S3. Absorption and SSHG spectra, $S(\lambda)$, measured with different concentrations of YOPRO-1 in PBS and at the dodecane/PBS interface.

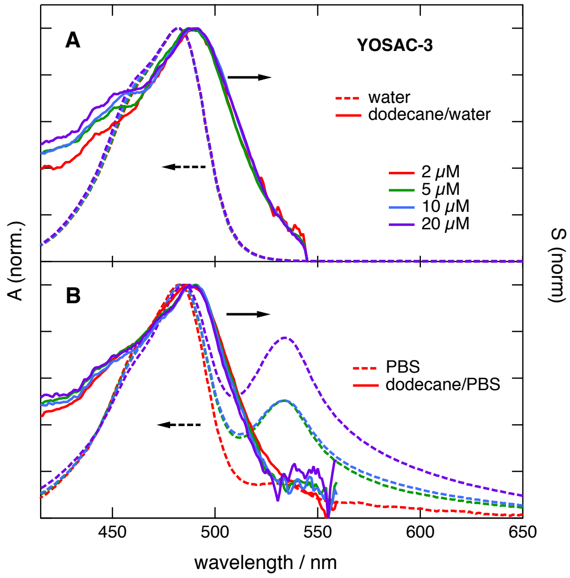

Figure S4. Absorption and SSHG spectra, $S(\lambda)$, measured with different concentrations of YOSAC-3 (A) in water and at the dodecane/water interface and (B) in PBS and at the dodecane/PBS interface.

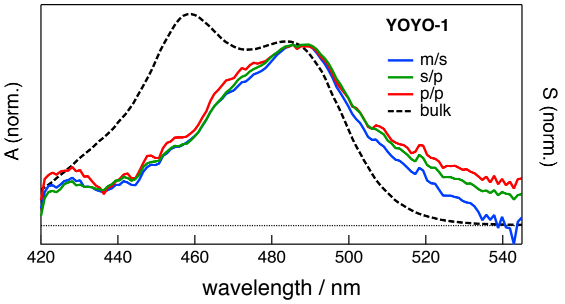

Figure S5. SSHG spectra measured at the dodecane/water interface with YOYO-1 (10 µM) at different polarization geometries. The electronic absorption spectrum is shown for comparison.

2. Orientation analysis

The nonlinear SSHG intensity (I_{SSHG}) at frequency 2ω under TIR condition can be expressed as:[S1-3]

$$I_{SSHG} = \frac{\omega^2}{8\varepsilon_0 c^3} \frac{\left(\varepsilon_1^{2\omega}\right)^{1/2}}{\varepsilon_1^{\omega}\left(\varepsilon_m^{2\omega} - \varepsilon_1^{\omega}\sin^2\theta_1^{\omega}\right)} \left|\chi^{(2)}\right|^2 I_{pr}^2 \tag{S1}$$

where $\varepsilon_{1,m}^{\omega}$ and θ_1^{ω} are the relative dielectric constants and the angle of incidence of the near-IR probe beam. In our case, the subscripts *1* and *m* refers to the upper dodecane phase and the dodecane/water interface, respectively. As mentioned in the main text, the macroscopic nonlinear optical susceptibility, $\tilde{\chi}^{(2)}$, is a second rank tensor containing 27 elements. However, in the case of isotropic interfaces, it contains only three independent nonzero elements:

$$\begin{aligned} I_{SSHG}(\gamma,\Gamma) = C\Big| & a_1\chi_{XXZ}^{(2)}\sin 2\gamma \sin\Gamma + \left(a_2\chi_{XXZ}^{(2)} + a_3\chi_{ZXX}^{(2)} \right. \\ & \left. + a_4\chi_{ZZZ}^{(2)}\right)\cos^2\gamma\cos\Gamma + a_5\chi_{ZXX}^{(2)}\sin^2\gamma\cos\Gamma\Big|^2 I_{pr}^2 \end{aligned} \tag{S2}$$

where γ and Γ are the polarization angles of the probe and the signal fields. The optical coefficients a_1-a_5 are determined from the relative dielectric constants of the different media and the angle of incidence. These coefficients were calculated as described in ref.[S1] using the following experimental values:

$$n_{1,dod} = 1.42;\ \ n_{2,buff} = n_{2,wat} = 1.33;\ n_m = 1.378$$

where n_m was calculated as the average of n_1 and n_2.[S4] Moreover no dispersion was assumed, i.e. the frequency dependence of the refractive indices was neglected. The Fresnel factors contained in the coefficients a_1-a_5 also depend on the angle of incidence of the probe field that was fixed experimentally at 70° (TIR).

Table S1. Coefficients determined from the refractive indices of the different media and the angle of incidence.

Coefficients	***Real part***	***Imaginary part***
a_1	5.37972	-5.84029
a_2	0.05387	-0.0627639
a_3	-0.026935	0.0313819
a_4	4.86507	-5.66829
a_5	5.37972	-5.84029

The polarization-resolved SSHG measurements were carried out at three different output polarizations, namely $\Gamma = 0^{\circ}$ (*p*), 45°, and 90° (*s*) ($\Gamma = 0°$), allowing the relative magnitude and sign of the three susceptibility elements previously introduced to be extracted. The following expressions can be obtained from eq.(S2):

$$I_{SSHG}\left(\gamma,0^{\circ}\right) \propto \left|\left(a_2\chi^{(2)}_{XXZ} + a_3\chi^{(2)}_{ZXX} + a_4\chi^{(2)}_{ZZZ}\right)\cos^2\gamma + a_5\chi^{(2)}_{ZXX}\sin^2\gamma\right|^2 \tag{S3a}$$

$$I_{SSHG}\left(\gamma,45^{\circ}\right) \propto \left|a_1\chi^{(2)}_{XXZ}\sin 2\gamma + \left(a_2\chi^{(2)}_{XXZ} + a_3\chi^{(2)}_{ZXX} + a_4\chi^{(2)}_{ZZZ}\right)\cos^2\gamma + a_5\chi^{(2)}_{ZXX}\sin^2\gamma\right|^2 \tag{S3b}$$

$$I_{SSHG}\left(\gamma,90^{\circ}\right) \propto \left|a_1\chi^{(2)}_{XXZ}\sin 2\gamma\right|^2 \tag{S3c}$$

These three equations can be used in a least-squares curve fitting analysis of the data shown in **Figure S6** and **S7** in order to obtain the ratios of the susceptibility elements listed in **Table S2**.

The macroscopic second-order nonlinear susceptibility depends on the hyperpolarizability tensor $\overleftrightarrow{\beta}$ as:

$$\overleftrightarrow{\chi}^{(2)} = \frac{1}{\varepsilon_0} N\langle T\rangle \overleftrightarrow{\beta} \tag{S4}$$

where $\langle T\rangle$ is a transformation tensor (averaging over all the orientations) from the molecular to the lab frame. The dyes studied here can be considered as axial molecules with a charge transfer character along the molecular axis (see molecular orbitals in **Figure S8**). In this case, one can assume that there is only one dominant element of the first hyperpolarizability tensor, the one aligned along the main molecular axis z, β_{zzz} (z being defined as the axis parallel to the transition dipole moment as shown **Figure 7**). Furthermore, the frequency-dependent calculations confirm this assumption, predicting only β_{zzz} as the dominant element. In this situation, the macroscopic susceptibility and microscopic hyperpolarizability are related to each other by the following relations:[S1]

$$\chi^{(2)}_{ZXX} = \chi^{(2)}_{XXZ} = \frac{1}{2} N \left\langle \sin^2\theta \cos\theta \right\rangle \beta_{zzz} \qquad \text{(S5a)}$$

$$\chi^{(2)}_{ZZZ} = N \left\langle \cos^3\theta \right\rangle \beta_{zzz} \qquad \text{(S5b)}$$

where θ is the tilt angle, i.e. the angle between the transition dipole moment and the normal at the interface (*Z-axis*).

The orientational parameter, D, can be expressed as:[S1,5-6]

$$D = \frac{\left\langle \cos^3\theta \right\rangle}{\left\langle \cos\theta \right\rangle} = \frac{\chi^{(2)}_{ZZZ}}{\chi^{(2)}_{ZZZ} + 2\chi^{(2)}_{ZXX}} \qquad \text{(S6)}$$

If one considers a infinitely narrow distribution of the angles at the interface, i.e. a Dirac distribution, eq.(S6) simplifies to $D = \cos^2\theta$. This latter approximation was used to extract the orientation angles reported in **Table S2**. In order to check if our assumption of one dominant hyperpolarizability element were true, we also performed an analysis of the polarization-resolved SSHG data assuming molecules with two main hyperpolarizability elements, namely β_{zzz} and β_{zxx}. In this case, it can be shown that:[S1]

$$\frac{\beta_{zzz}}{\beta_{zxx}} = \frac{\chi^{(2)}_{ZZZ} + 2\chi^{(2)}_{XZX}}{2\left(\chi^{(2)}_{ZXX} - \chi^{(2)}_{XZX}\right)} \tag{S7}$$

These ratios are reported in **Table S2** together with the orientational angles. As one can see, the ratio is clearly larger than 1 for all the molecules, confirming that β_{zzz} is truly the dominant element in the hyperpolarizability tensor. Similar results were obtained assuming β_{zzz} and β_{xxz} as the main elements:[S1]

$$\frac{\beta_{zzz}}{\beta_{xxz}} = \frac{\chi^{(2)}_{ZZZ} + 2\chi^{(2)}_{ZXX}}{2\left(\chi^{(2)}_{XXZ} - \chi^{(2)}_{ZXX}\right)} \tag{S8}$$

The polarization profiles shown in **Figures S6** and **S7** exhibit around 270° a small deviation from the values measured at 90°. It originates from a defect of the half-wave plate used to rotate the fundamental polarization. This affects only slightly the error in the fitting procedure.

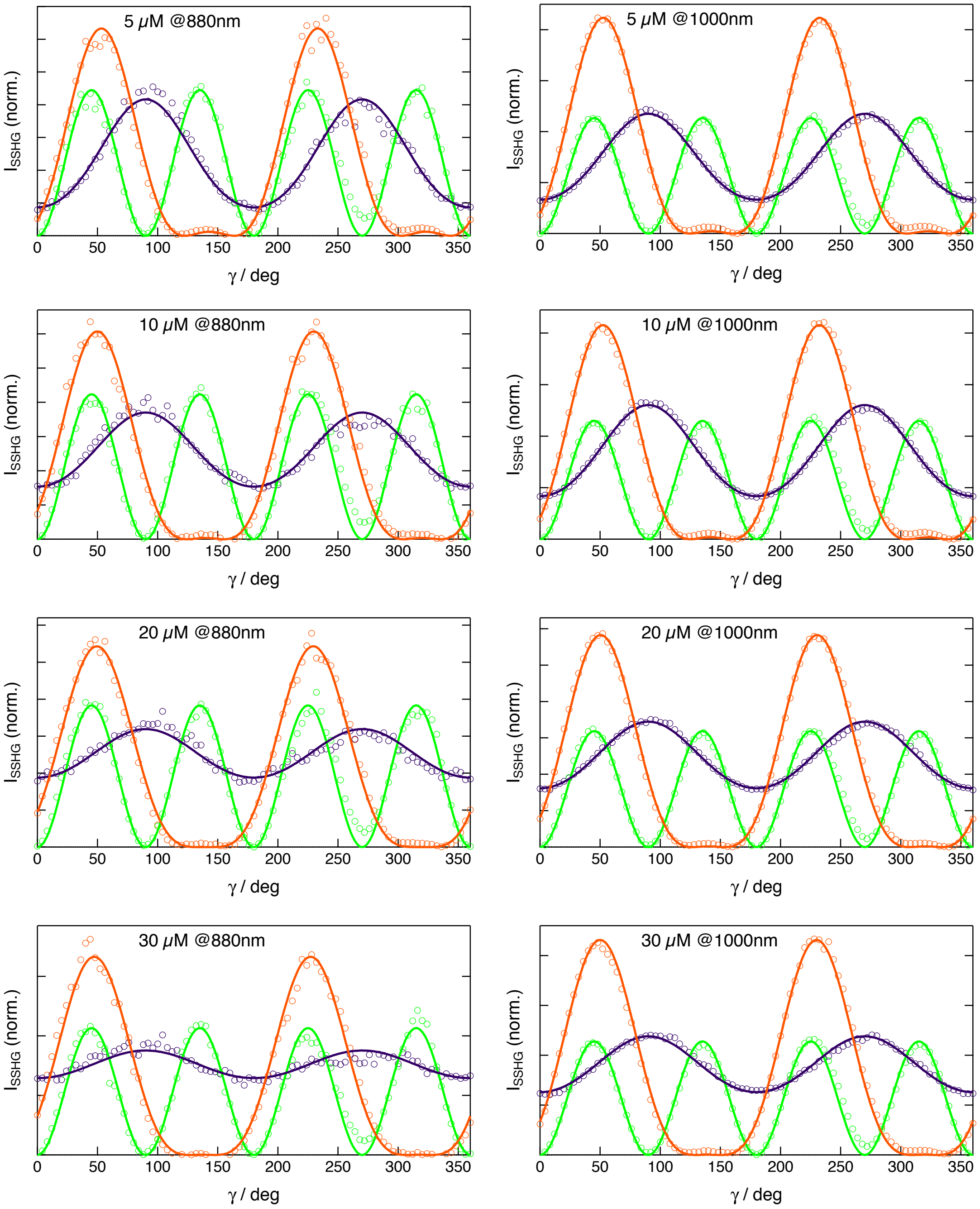

Figure S6. Polarization profiles measured with YOYO-1 at different concentrations and recorded at $\Gamma = 0^{\circ}$ (p, black), $\Gamma = 90^{\circ}$ (s, green) and $\Gamma = 45^{\circ}$ (orange) upon probing at 880 and 1000 nm.

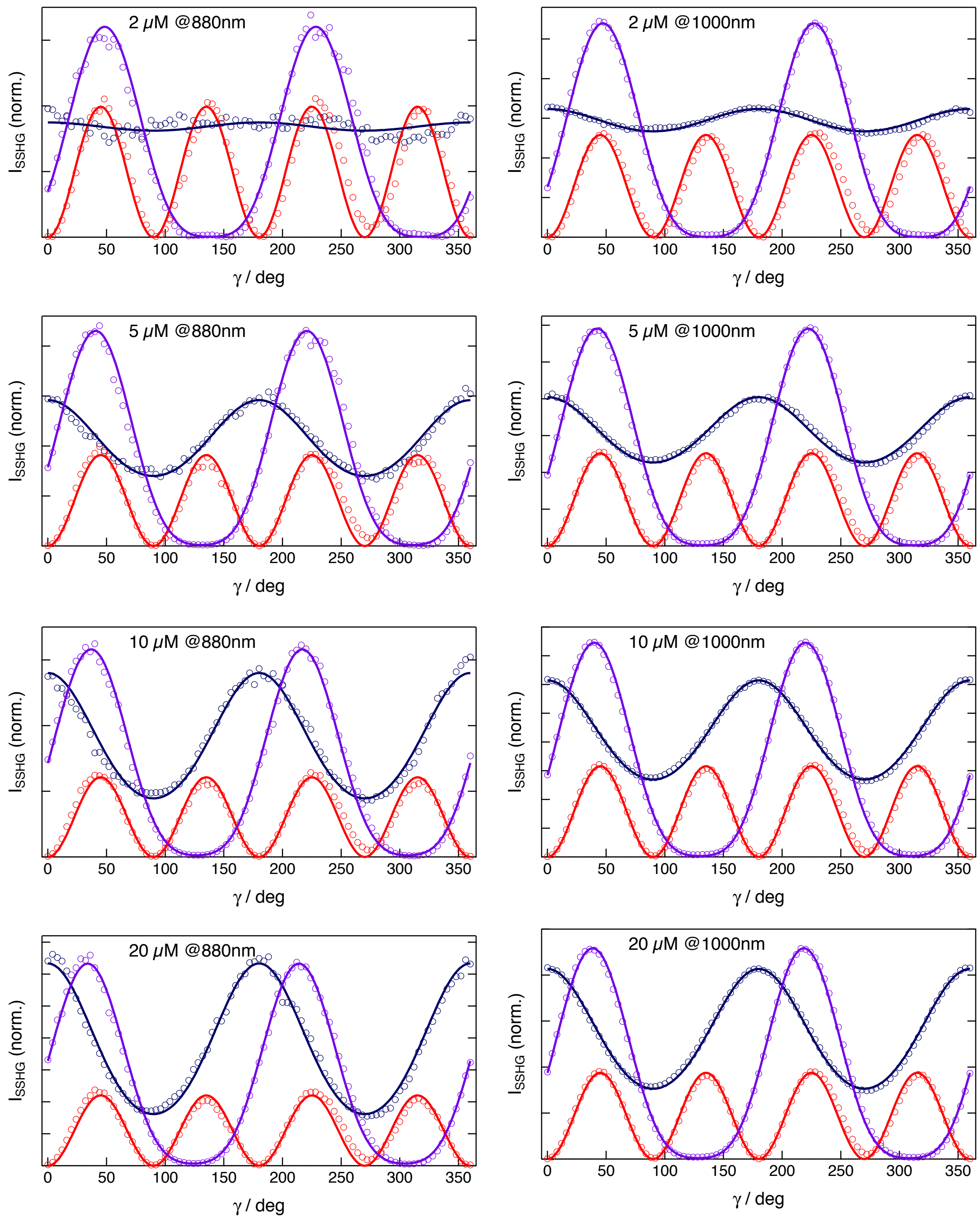

Figure S7. Polarization profiles measured with YOSAC-1 at different concentrations and recorded at $\Gamma = 0^\circ$ (*p*, black), $\Gamma = 90^\circ$ (*s*, red) and $\Gamma = 45^\circ$ (violet) upon probing at 880 and 1000 nm.

Table S2. Results from the analysis of the polarization-resolved SSHG data measured with YOYO-1 and YOSAC-1. The error is calculated from the fit with 99% confident interval and propagated through the various equations. The *D* parameters were calculated assuming one dominant susceptibility tensor (as confirmed also by QM calculation) and the tilt angles were deduced assuming a Dirac distribution. The relative sign of the three non-zero and independent susceptibility elements and the ratios $\left|\beta_{zzz}/\beta_{zxx}\right|$ and $\left|\beta_{zzz}/\beta_{xxz}\right|$ assuming two dominant elements, are also listed.

C* / *μM	***λ* / *nm***	$\chi^{(2)}_{ZXX}/\chi^{(2)}_{XXZ}$	$\chi^{(2)}_{ZZZ}/\chi^{(2)}_{XXZ}$	***D***	***θ* / deg**	$\left|\beta_{zzz}/\beta_{zxx}\right|$	$\left|\beta_{zzz}/\beta_{xxz}\right|$
YOYO-1							
5	880	+0.97 ± 0.02	+0.46 ± 0.02	0.19 ± 0.01	63.9 ± 0.9	2.3	37
	1000	+1.02 ± 0.01	+0.57 ± 0.01	0.22 ± 0.01	62.1 ± 0.3	3.0	71
10	880	+0.93 ± 0.02	+0.63 ± 0.02	0.25 ± 0.01	59.8 ± 0.9	3.6	19
	1000	+1.06 ± 0.01	+0.64 ± 0.01	0.23 ± 0.01	61.3 ± 0.3	3.6	21
20	880	+0.91 ± 0.02	+0.74 ± 0.02	0.29 ± 0.01	57.5 ± 0.9	5.2	15
	1000	+1.04 ± 0.01	+0.75 ± 0.01	0.27 ± 0.01	59.0 ± 0.4	5.5	35
30	880	+0.91 ± 0.02	+0.82 ± 0.01	0.31 ± 0.02	56.1 ± 1.0	802	14
	1000	+1.02 ± 0.01	+0.79 ± 0.01	0.28 ± 0.01	58.2 ± 0.5	6.5	64
YOSAC-1							
2	880	+0.90 ± 0.03	+0.99 ± 0.03	0.35 ± 0.02	53.5 ± 1.0	>100	15
	1000	+1.02 ± 0.02	+1.18 ± 0.03	0.37 ± 0.01	52.7 ± 0.4	8.6	93
5	880	+0.88 ± 0.02	+1.34 ± 0.02	0.43 ± 0.01	48.9 ± 0.7	4.9	13
	1000	+0.95 ± 0.01	+1.34 ± 0.02	0.41 ± 0.01	50.1 ± 0.4	4.9	32
10	880	+0.86 ± 0.02	+1.61 ± 0.03	0.48 ± 0.01	45.9 ± 0.8	3.0	12
	1000	+0.92 ± 0.01	+1.48 ± 0.01	0.44 ± 0.01	48.2 ± 0.3	3.7	22
20	880	+0.86 ± 0.02	+1.80 ± 0.03	0.51 ± 0.01	44.3 ± 0.7	2.4	12
	1000	+0.90 ± 0.01	+1.57 ± 0.01	0.46 ± 0.01	47.0 ± 0.4	3.1	17

3. Quantum mechanical calculations

Quantum-chemistry calculations were only performed to obtain qualitative information on the second-order nonlinear optical response of YO monomers and dimers. For this, it is strongly recommended to use a method that adequately represents the electronic excitations because the second-order nonlinear optical response is closely related to the charge-transfer (CT) character of the excited-states.[S7] We have used the CAM-B3LYP functional that is known to give better results for estimating CT excitations. Nevertheless, we have obtained a first vertical transition for YO that is around 0.4 V blue-shifted relatively to the experimental value.[S8] However, it has been pointed out in the literature that the "0.1 eV rule of thumb" between measured absorption maximum and computed vertical transition is not always valid.[S9] It does not apply for example if the valence transition is nonvertical and too anharmonic. Therefore, the modeling used throughout is more than acceptable for a qualitative comparison of monomer and dimers.

Table S3. Vertical excitation energies to the first singlet excited state of YO and to the two excitonic states of the H- and J-dimers and corresponding oscillator strength, *f*.

Species	*Singlet Ex. State*	*Energy / eV (nm)*	*f*	*Major MO contribution*
YO monomer	1	2.998 (413.6)	1.059	HOMO -> LUMO (98%)
H-dimer	1	2.904 (427.0)	0.050	HOMO -> LUMO (57.4%) HOMO-1 -> LUMO+1 (57.4%)
	2	3.077 (402.9)	1.863	HOMO -> LUMO+1 (48.1%) HOMO-1 -> LUMO (49.5%)
J-dimer	1	2.973 (417.0)	1.835	HOMO-1 -> LUMO (32.3%) HOMO -> LUMO+1 (30.9%) HOMO -> LUMO (17.2%) HOMO-1 -> LUMO+1 (17.0%)
	2	3.022 (410.3)	0.269	HOMO -> LUMO+1 (35.0%) HOMO-1 -> LUMO (34.8%) HOMO -> LUMO (14.4%) HOMO-1 -> LUMO+1 (13.4%)

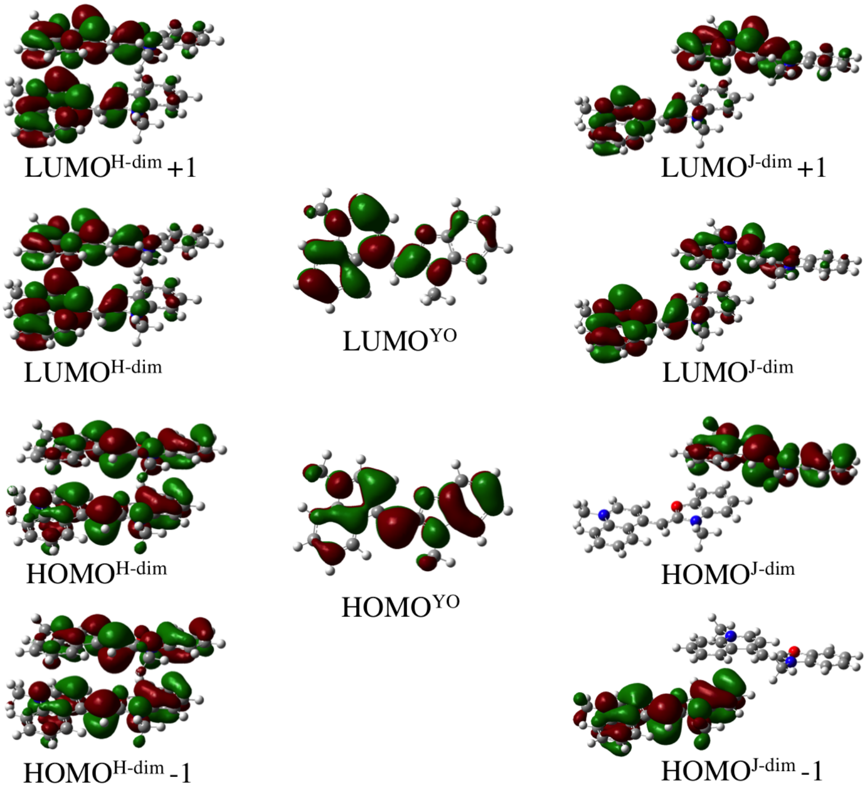

Figure S8. Frontier molecular orbitals drawn at the 0.02 a.u. level.

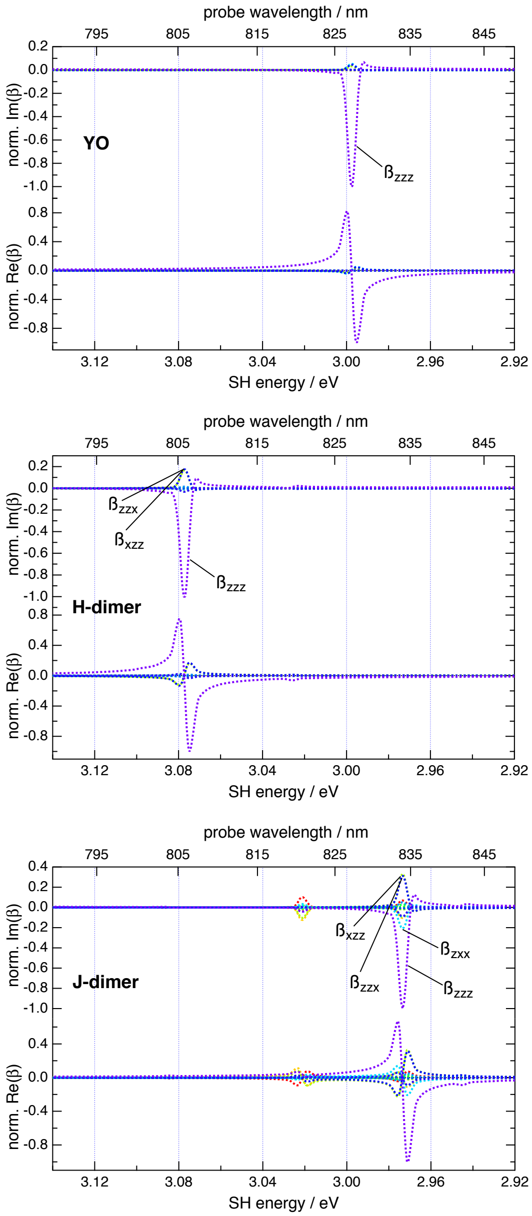

Figure S9. Full frequency-dependent hyperpolarizability tensor (18 elements for SHG) calculated for the YO, H-dimer and J-dimer models. The real and imaginary parts are plotted and the most intense resonant elements are indicated.

Table S4. Additional calculations of the hyperpolarizability in the static limit. The absolute values are in a.u. (1 a.u. = $8.639 \cdot 10^{-33}$ cm^5 esu^{-1}).

β element ω (0;0,0)	YO monomer	$\lvert\beta_{ijk}/\beta_{zzz}\rvert$	H-dimer	$\lvert\beta_{ijk}/\beta_{zzz}\rvert$	J-dimer	$\lvert\beta_{ijk}/\beta_{zzz}\rvert$
β_{xxx}	-307	*0.02*	65	*0*	5955.3	*0.41*
β_{xxy}	0	*0*	-204	*0.01*	-1081.3	*0.07*
β_{yxy}	-111	*0.01*	-159	*0.01*	-11.5	*0*
β_{yyy}	0	*0*	15	*0*	11.5	*0*
β_{xxz}	1180	*0.09*	-1274	*0.06*	-4757.6	*0.33*
β_{yxz}	0	*0*	566	*0.03*	1193.8	*0.08*
β_{yyz}	29	*0*	-179	*0.01*	-215.1	*0.01*
β_{zzx}	4390	*0.32*	10958	*0.52*	7885.7	*0.55*
β_{zyz}	-1	*0*	-1433	*0.07*	-974.5	*0.07*
β_{zzz}	-13653	*1.00*	-21121	*1.00*	-14418.3	*1.00*

4. Additional TR-SSHG data

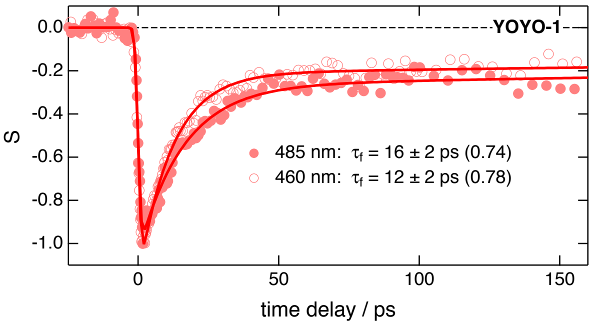

Figure S10. TR-SSHG profiles, *S*(*t*), measured at 460 and 485 nm nm with YOYO-1 (10 μM) at the dodecane/water interface using *s*/*p* polarization geometry at 500 nm excitation. The solid lines are the best bi-exponential fits (τ_f is the time constant of the fast component and its relative amplitude is given in parentheses; the time constant of the slow component is > 1 ns).

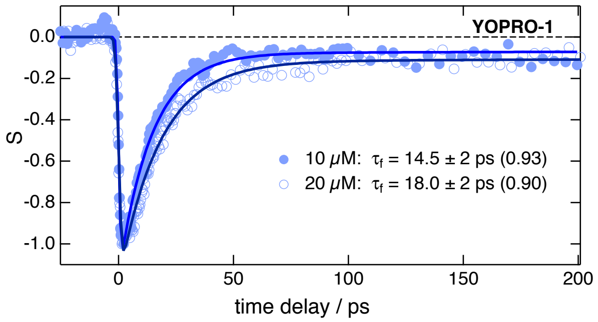

Figure S11. TR-SSHG profiles, *S*(*t*), measured at 485 nm with two different concentrations of YOPRO-1 at the dodecane/PBS interface using *s*/*p* polarization geometry at 500 nm excitation. The solid lines are the best bi-exponential fits (τ_f is the time constant of the fast component and its relative amplitude is given in parentheses; the time constant of the slow component is > 1 ns).

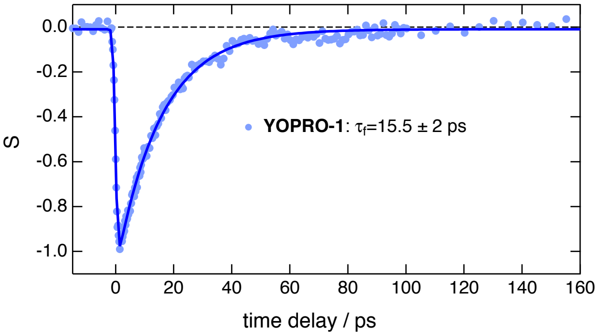

Figure S12. TR-SSHG profile, *S*(*t*), measured at 475 nm with YOPRO-1 (10 μM) at the dodecane/PBS with *m*/*s* polarization geometry upon 500 nm excitation and best monoexponential fit.

5. Silver mirror reflectance

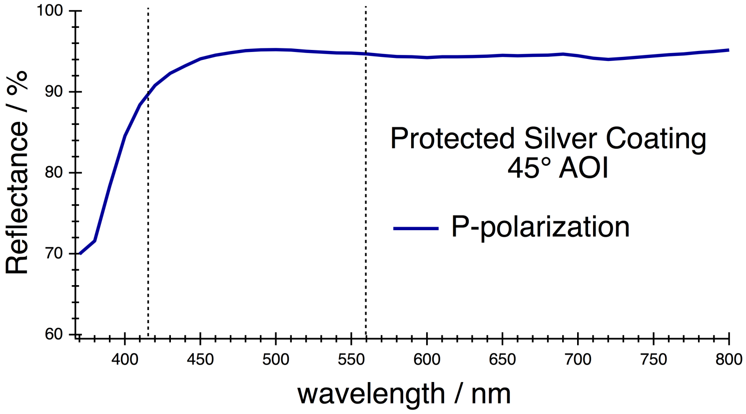

Figure S11. Reflectance of the silver mirror used as reference in the SSHG spectra measurements. The wavelength range used in this study is indicated by the two vertical dashed lines.

6. References

(S1) Brevet, P.-F. *Surface Second Harmonic Generation*; Presses polytechniques et universitaires romandes: Lausanne, 1997.

(S2) Nagatani, H.; Piron, A.; Brevet, P.-F.; Fermin, D. J.; Girault, H. H. Surface Second Harmonic Generation of Cationic Water-Soluble Porphyrins at the Polarized Water|1,2-Dichloroethane Interface *Langmuir* **2002**, *18*, 6647-6652.

(S3) Rinuy, J.; Piron, A.; Brevet, P. F.; Blanchard-Desce, M.; Girault, H. H. Intramolecular Electron Density Redistribution Upon Hydrogen Bond Formation in the Anion Methyl Orange at the Water/1,2-Dichloroethane Interface Probed by Phase Interference Second Harmonic Generation *Chem. Eur. J.* **2000**, *6*, 3434-3441.

(S4) Wang, H.; Borguet, E.; Eisenthal, K. B. Generalized Interface Polarity Scale Based on Second Harmonic Spectroscopy *J. Phys. Chem. B* **1998**, *102*, 4927.

(S5) Zhang, W.-K.; Wang, H.-F.; Zheng, D.-S. Quantitative Measurement and Interpretation of Optical Second Harmonic Generation from Molecular Interfaces *Phys. Chem. Chem. Phys.* **2006**, *8*, 4041-4052.

(S6) Rao, Y.; Tao, Y.-s.; Wang, H.-f. Quantitative Analysis of Orientational Order in the Molecular Monolayer by Surface Second Harmonic Generation *J. Chem. Phys.* **2003**, *119*, 5226.

(S7) Kanis, D. R.; Ratner, M. A.; Marks, T. J. Design and Construction of Molecular Assemblies with Large Second-Order Optical Nonlinearities. Quantum Chemical Aspects *Chem. Rev.* **1994**, *94*, 195-242.

(S8) Carlsson, C.; Larsson, A.; Jonsson, M.; Albinsson, B.; Norden, B. Optical and Photophysical Properties of the Oxazole Yellow Probes Yo and Yoyo *J. Phys. Chem.* **1994**, *98*, 10313-10321.

(S9) Lasorne, B.; Jornet-Somoza, J.; Meyer, H. D.; Lauvergnat, D.; Robb, M. A.; Gatti, F. Vertical Transition Energies Vs. Absorption Maxima: Illustration with the Uv Absorption Spectrum of Ethylene *Spectrochim. Acta A* **2014**, *119*, 52-58.